



HAL
open science

New $\text{P2-Na}_{0.70}\text{Mn}_{0.60}\text{Ni}_{0.30}\text{Co}_{0.10}\text{O}_2$ layered oxide as electrode material for Na-ion batteries

Jun Yoshida, Elodie Guérin, Mélissa Arnault, Cédric Constantin, Benoit Mortemard de Boisse, Dany Carlier, Marie Guignard, Claude Delmas

► To cite this version:

Jun Yoshida, Elodie Guérin, Mélissa Arnault, Cédric Constantin, Benoit Mortemard de Boisse, et al.. New $\text{P2-Na}_{0.70}\text{Mn}_{0.60}\text{Ni}_{0.30}\text{Co}_{0.10}\text{O}_2$ layered oxide as electrode material for Na-ion batteries. Journal of The Electrochemical Society, 2014, 161 (14), pp.A1987-A1991. 10.1149/2.0121414jes . hal-01080502

HAL Id: hal-01080502

<https://hal.science/hal-01080502>

Submitted on 24 Jun 2022

HAL is a multi-disciplinary open access archive for the deposit and dissemination of scientific research documents, whether they are published or not. The documents may come from teaching and research institutions in France or abroad, or from public or private research centers.

L'archive ouverte pluridisciplinaire **HAL**, est destinée au dépôt et à la diffusion de documents scientifiques de niveau recherche, publiés ou non, émanant des établissements d'enseignement et de recherche français ou étrangers, des laboratoires publics ou privés.

New P2 - Na_{0.70}Mn_{0.60}Ni_{0.30}Co_{0.10}O₂ Layered Oxide as Electrode Material for Na-Ion Batteries

Jun Yoshida,^{a,b} Elodie Guerin,^a Mélissa Arnault,^a Cédric Constantin,^a Benoit Mortemard de Boisse,^a Dany Carlier,^a Marie Guignard,^a and Claude Delmas^{a,z}

^aICMCB-CNRS, Bordeaux, 33608 Pessac, France

^bTOYOTA MOTOR EUROPE NV/SA, B-1930 Zaventem, Belgium

Sodium layered oxide, Na_{0.70}Mn_{0.60}Ni_{0.30}Co_{0.10}O₂, with a P2-type structure was synthesized by a co-precipitation method and characterized as positive electrode of sodium batteries. The P2-Na_xMn_{0.60}Ni_{0.30}Co_{0.10}O₂ electrode delivered a high specific capacity of 185 mAh/g in the 1.5–4.3 V range at 1st cycle at C/20 rate; however, rapid capacity decay is observed. In the 1.7–4.0 V range the capacity is equal to 125 mAh/g with a fading considerably reduced. The rate capability is reasonably good. According to the electrochemical profile, a potential plateau around 4.2 V vs. Na⁺/Na, meaning a bi-phasic domain, and several voltage drops that could be related to single phase domains in a narrow sodium content range are observed. Even if the capacity decreases when the battery is cycled above 4.0 V, there is no irreversible structural change.

Owing to abundant sodium resource and therefore the low price of sodium compounds, sodium-ion batteries are thought to be one of favorite future batteries for hybrid vehicles (HVs). Recently, a rapid expansion of the HVs market is inducing to grow lithium consumption. Therefore, to face lack of lithium resource problem, it is necessary to develop sodium-ion battery technology. Concerning positive electrode materials, Na_xMO₂ layered type phase have been studied for a long time. They were first studied in the 80's by Delmas et al.^{1–3} Layered Na_xMO₂ are classified into several groups denoted such as P2 or O3. The letter indicates the site environment of sodium with oxygen (prismatic or octahedral) and the number indicates the number of MO₂ slabs within the hexagonal cell.⁴ For instance in the P2 type structure, we focus on in this study, sodium ions are in trigonal prismatic sites between two MO₂ slabs with different orientations. In the 2000's many studies were performed in Dahn's group on P2-Na_{2/3}Ni_{1/3}Mn_{2/3}O₂ phases and their cobalt substituted derivatives.^{5–8} These authors characterized these materials and used them as precursors for the syntheses of new lithium phases obtained by exchange reactions. For several years, thanks to the potential interest of sodium-ion batteries, a huge number of researches are carried out on layered sodium oxides and in particular on P2 type phases.^{9–12}

The higher ion diffusivity in trigonal prismatic environment vs. octahedral one¹³ led several researchers to report that P2-type structure leads to higher capacity and cyclability than the O3 one. Yabuuchi et al. reported that P2-Na_{2/3}Fe_{1/2}Mn_{1/2}O₂ exhibits a capacity for the first cycle of 190 mAh/g, which was higher than that of reported O3 (100–110 mAh/g).¹⁴ Some of us discussed electrochemical performances between P2 and O3 structure types for Na_xMn_{1-y}Fe_yO₂, and they deduced that those of P2-type material were better than those of O3-type one.¹⁵ Other authors reported on different phases with P2-type structure: Na_xFe_yMn_{1-y}O₂,¹⁶ Na_{2/3}Ni_{1/3}Mn_{2/3}O₂,^{5,17,18} Na_{2/3}Co_{2/3}Mn_{1/3}O₂¹⁹ and Na_{0.70}Mn_{0.11}Co_{0.89}O_{2+z},²⁰ for example, which exhibit interesting electrochemical behavior. P2 type structure with three transition metals, such as Na_{2/3}Co_xNi_{1-x}Mn_{2/3}O₂,^{6,7} Na_{0.45}Ni_{0.22}Co_{0.11}Mn_{0.66}O₂,²¹ Na_{0.67}Mn_{0.65}Co_{0.20}Ni_{0.15}O₂,²² Na_{2/3}Co_{2/3}Ni_{1/9}Mn_{2/9}O₂²³ have been investigated in order to improve the electrochemical performances by analogy with lithium-based materials as LiMn_{1/3}Ni_{1/3}Co_{1/3}O₂.²⁴ Yuan et al. recently reported on a Na_{0.67}Mn_{0.65}Fe_{0.20}Ni_{0.15}O₂ material, which delivers a high specific capacity of 208 mAh/g in the 1.5–4.3 V range vs. Na⁺/Na.²⁵ In this work, we focus on the Na_{0.70}Mn_{0.60}Ni_{0.30}Co_{0.10}O₂ composition obtained by a co-precipitation method. Its crystal structure and morphology are characterized using X-ray diffraction (XRD) and scanning electron microscopy (SEM); electrochemical properties were also examined in Na cells.

Experimental

Synthesis methods.— A co-precipitation method is used to make the aimed compound. Two solutions, one made of Co(NO₃)₂ · 6H₂O, Ni(NO₃)₂ · 6H₂O and Mn(NO₃)₂ · 4H₂O (one mole/l of the transition metal ions with the selected composition), and another one made of Na₂CO₃ (one mole/l), were simultaneously dropped into a beaker with 450 ml of distilled water by using a syringe pusher with a flow of 50 ml/min, with stirring at 700 rpm and keeping at 50°C. Therefore, all along the precipitation the target material stoichiometry and the pH was maintained. The precipitate thus formed was washed with distilled water 5 times, and dried at 80°C for two days. The dried powder was mixed with Na₂CO₃ in a glove box filled under argon to reach the Na_{0.70}Mn_{0.60}Ni_{0.30}Co_{0.10}O₂ composition. A 10 wt% excess of Na₂CO₃ was added to compensate its volatility at high temperature. The mixture was calcinated at 600°C for 6 hours, and then heated at 900°C for 12 hours in air or in oxygen. Finally, it was quenched in air down to room temperature. Preliminary experiments have shown that there is no difference either from a structural nor an electrochemical point of view when the syntheses were realized under air or oxygen.

Characterization.— Powder XRD patterns were recorded on a powder diffractometer (D5000, Bruker or Enpyrean, Panalytical) equipped with a Cu target (Cu $\alpha_{1,2}$). The measurement was carried out from 10° to 80° with steps of 0.02°; the total acquisition time was 14 h 30. To prevent the effect of water, all the XRD experiments were done in a homemade air-tight sample holder. The cell parameter refinement was performed with LeBail method in FullProf program.²⁶ Morphological images were observed on a Hitachi S4500 field emission scanning electron microscope (SEM) with an accelerating voltage of 3.0 kV. Gold coating was implemented before the observations. The electrochemical performances were evaluated in two electrodes configuration using metallic sodium as the counter electrode in Swagelok or coin type cells. The positive electrode was a mixture containing 88 wt% of the active material, 10 wt% of carbon black as electronic conductor and 2 wt% of polytetrafluoroethylene (PTFE) as binder. The electrolyte was 1 M NaPF₆ (Alfa Aesar 99%) in propylene carbonate (Sigma Aldrich anhydrous 99%) with 2 wt% of fluoroethylene carbonate (FEC) as additive. Galvanostatic performances were evaluated at the C/20 current rate at 25°C. All cell voltages are given vs Na⁺/Na redox couple.

Results

Material syntheses and characterization.— A systematic study of several compositions was made to obtain P2 type phases with the Na_x(Mn,Ni,Co)O₂ formula. The amount of sodium was selected equal to 0.70 that is the classical sodium amount to obtain this structural type; this leads to an average transition metal oxidation state equal

^zE-mail: delmas@icmcb-bordeaux.cnrs.fr

Table I. Various tested compositions to obtain pure P2 type phase.

Composition	Theoretical Ni ³⁺ amount	Obtained material	Relative NiO amount
Na _{0.70} Mn _{0.30} Ni _{0.425} Co _{0.275} O ₂	0.425	P2 + NiO	VL
Na _{0.75} Mn _{0.30} Ni _{0.425} Co _{0.275} O ₂	0.375	P2 + NiO	VL
Na _{0.80} Mn _{0.30} Ni _{0.425} Co _{0.275} O ₂	0.325	P2 + NiO	L
Na _{0.70} Mn _{0.35} Ni _{0.275} Co _{0.375} O ₂	0.225	P2 + NiO	L
Na _{0.75} Mn _{0.35} Ni _{0.275} Co _{0.375} O ₂	0.175	P2 + NiO	M
Na _{0.80} Mn _{0.35} Ni _{0.275} Co _{0.375} O ₂	0.125	P2 + NiO	M – S
Na _{0.70} Mn _{0.425} Ni _{0.425} Co _{0.15} O ₂	0.30	P2 + NiO	L
Na _{0.90} Mn _{0.425} Ni _{0.425} Co _{0.15} O ₂	0.10	P2 + O3 + NiO	S
Na _{0.70} Mn _{0.60} Ni _{0.30} Co _{0.10} O ₂	0	P2	-

(VL : Very large, L : Large, M : Medium, S : Small)

to 3.3. Then, the relative amount of transition metals was determined having in mind the relative stability of the various redox couples: (i) Mn³⁺ and Ni³⁺ cannot be simultaneously present as Mn³⁺ + Ni³⁺ gives spontaneously Mn⁴⁺ + Ni²⁺ via an internal redox reaction, (ii) Co⁴⁺ is no longer stable in front of Ni²⁺. All tests with various compositions satisfying the previous requirements, but containing Ni³⁺ were unsuccessful whatever the experimental conditions; NiO was present in all samples. Table I gives a summary of the various experiments which have been done. It clearly appears that when the theoretical amount of Ni³⁺ decreases the amount of NiO experimentally found in the sample as an impurity decreases. In the literature, all P2 type materials with general formula Na_x(Mn,Ni,Co)O₂ satisfy the previous requirements. They can contain Mn³⁺, Mn⁴⁺, Co³⁺ and Ni²⁺; but never Ni³⁺.^{7,8,23} Therefore, we selected compositions with no trivalent Ni³⁺ with general formula: Na_{0.70}Mn_{0.3+x}Ni_xCo_{0.7-x}O₂. In this case, materials with the P2 type structure were obtained as pure phases. This behavior seems to be related to the stability of the P2 structure as in the case of the lithium O3 phases, Ni³⁺ and Ni²⁺ can be simultaneously present (Li_{1.12}Mn_{0.37}Ni_{0.37}Co_{0.13}O₂ for example).²⁷ Further studies are required to understand this behavior. Among all possible compositions we focused our study on the Na_{0.70}Mn_{0.60}Ni_{0.30}Co_{0.10}O₂ composition which contains a small amount of expensive cobalt. This phase was obtained in air at 900°C as described in the experimental part. Its XRD powder pattern is shown in Fig. 1. The profile was refined in the hexagonal system with the classical space group of the P2 type phase (P6₃/mmc). All diffraction lines are indexed that shows that no impurities can be detected by XRD. The cell parameters are a_{hex.} = 2.8842(1) Å, and c_{hex.} = 11.089(1) Å. Images of the particles are given in Fig. 2. They illustrate that average diameter of primary and secondary particles are around 1–2 μm and 60 μm, respectively. The primary particles have hexagonal shape, which is typical in the layered materials.

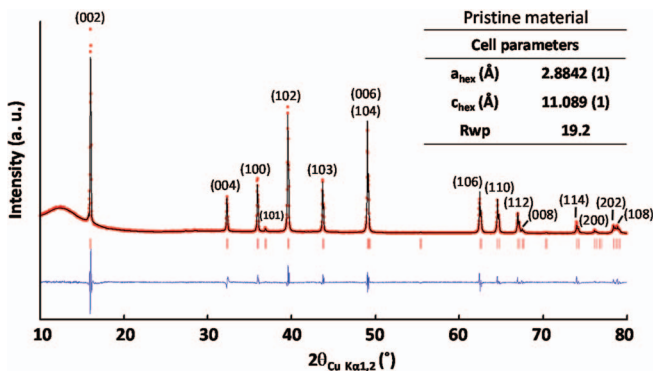


Figure 1. XRD pattern of the Na_{0.70}Mn_{0.60}Ni_{0.30}Co_{0.10}O₂ phase synthesized by a co-precipitation method: (black) full pattern matching pattern, (red) experimental data, (blue) difference plots.

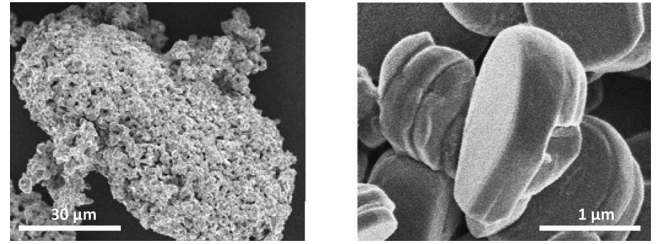


Figure 2. SEM images of P2-Na_{0.70}Mn_{0.60}Ni_{0.30}Co_{0.10}O₂ powder.

Electrochemical behavior.— Galvanostatic cycling curve of a Na//Na_{0.70}Mn_{0.60}Ni_{0.30}Co_{0.10}O₂ (C/20 rate) cell is shown in Fig. 3a. The specific capacity is equal to 185 mAh/g at the 1st cycle when the battery is cycled in the 1.5–4.3 V range. A small shift is observed between the first and the second charge that may result from electrolyte oxidation in relation with the formation of the solid electrolyte interphase (SEI) involving the FEC additive.²⁸

The effect of the upper and lower voltage cut-off values has been also studied. As shown in Fig. 3b and 3c, cycling the battery in the 1.5–4.0 V and 1.7–4.0 V voltage ranges limits significantly the capacity fading in comparison to that in the 1.5 V–4.3 V range. Fig. 4 shows the comparison of the discharge capacity evolutions along with the cycling number. It can be noticed that the capacity retention given in

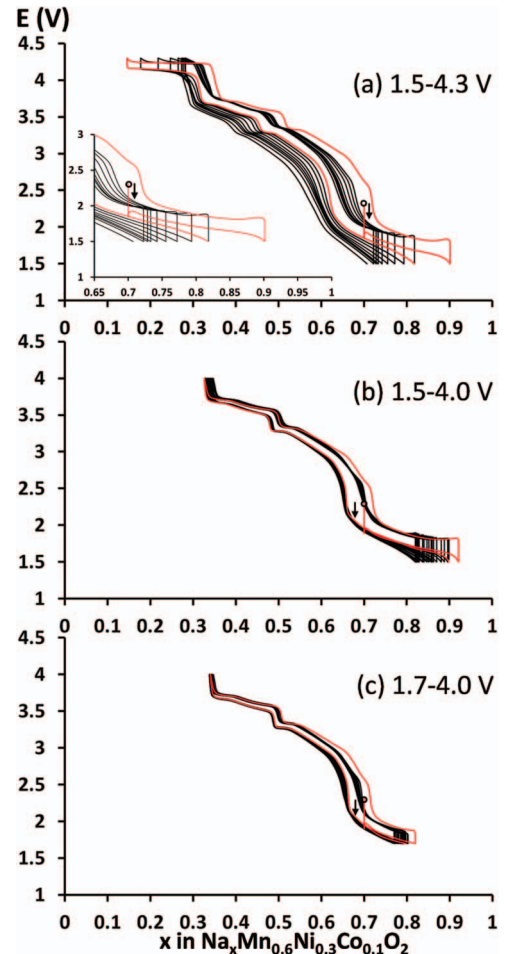


Figure 3. Galvanostatic curves of Na//P2-Na_{0.70}Mn_{0.60}Ni_{0.30}Co_{0.10}O₂ at C/20 in various voltage ranges. The black dot indicates the initial voltage. (a) in 1.5–4.3 V. A magnification around the initial point is shown in the inset. (b) 1.5–4.0 V. (c) 1.7–4.0 V. The first discharge and the following first cycle are represented by the red line.

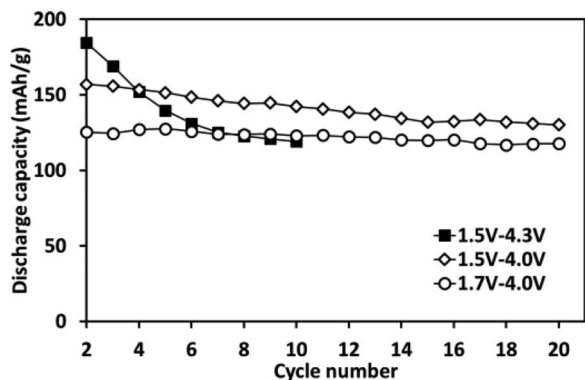


Figure 4. Change in specific capacity upon cycling of Na//P2-Na_{0.70}Mn_{0.60}Ni_{0.30}Co_{0.10}O₂ in various voltage ranges.

the 1.7–4.0 V range is approximately 94%, which is higher than those in the other voltage ranges (82% in 1.5–4.0 V, 58% in 1.5–4.3 V). In the 1.7–4.0 V range the shape of the curve is not modified at all that emphasizes the reversibility of the intercalation/deintercalation reaction in this voltage range.

The rate capability test was performed from C/20 to C during a cycling in the 1.7–4.0 V range. At each rate three cycles were done. At the end of the experiment, three cycles at C/20 were also done for comparison. As shown in Fig. 5 the capacity decreases from 120 mAh/g at C/20 to 80 mAh/g at C and return to 127 mAh/g when the rate comes back to C/20. A slight increase is even observed, which can result from an activation of the material. No material activation is observed during the C/20 cycling in the same voltage range. One can assume that at high rate, there are large concentration gradients that induce constraints within the particles. A chemical grinding of the primary particles or an increase of the porosity of the secondary particles could improve the reaction kinetics and therefore, increase the cell capacity.

The shape of the curve shows the existence on several parts separated by rapid changes in voltage. In a first step the battery was discharged to 1.5 V. This initial discharge profile, given in the inset of Fig. 3a, indicates that sodium ions can be inserted up to $x = 0.90$, not reaching the full occupancy for the sodium sites that is a general phenomenon occurring in layered materials. In this part of the discharge it is assumed that only the Mn⁴⁺/Mn³⁺ redox couple is active: Mn⁴⁺ ions are reduced to Mn³⁺ to compensate Na⁺ intercalation. Nevertheless, further experiments are required to prove that cobalt ions are not partially reduced to the divalent state as we have previously reported in the case of the P2-Na_xCo_{2/3}Mn_{1/3}O₂ system.^{19,29}

During the battery charge above 2.30 V, which corresponds to the open circuit voltage of the starting battery, one observes a continuous variation of the cell voltage with two voltage drops at $x \approx 0.5$ and $x \approx 0.35$ that indicate the existence of specific compositions partic-

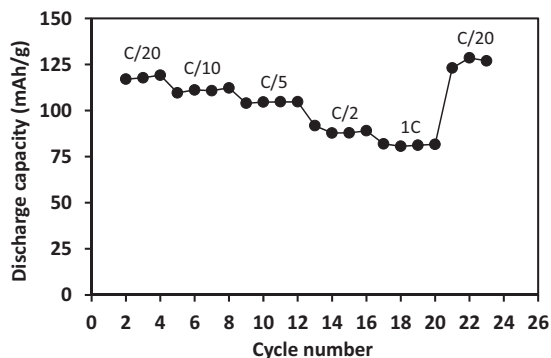


Figure 5. Effect of the cycling rate on the specific capacity.

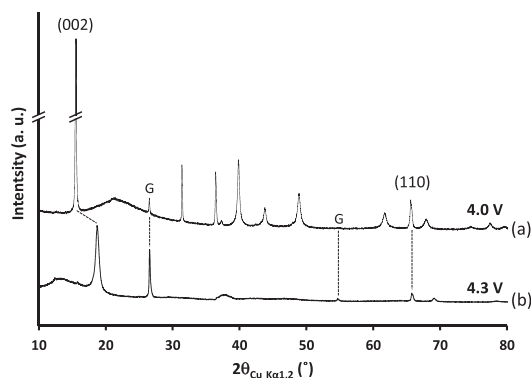


Figure 6. XRD patterns of the material recovered on both sides of the plateau. (a) After charge at 4.0 V; (b) After charge at 4.3 V. G: graphite.

ularly stable in a narrow sodium content range. It is assumed that these voltage drops are related to the occurrence of sodium / vacancy orderings between the MO₂ slabs. Such a behavior is generally not observed in a multication slab composition. In general, the cationic disorder within the slab prevents any sodium ordering in the interslab space. From the redox point of view it is assumed that for $x < 0.7$, Ni²⁺ are oxidized to Ni³⁺ in a first step then to Ni⁴⁺. Cobalt oxidation has also to be considered. In the case of P2-Na_xCoO₂ system, Co⁴⁺ ions are observed in the whole voltage range between 2.3–3.8 V range.³⁰ In addition, like in lithium systems, the oxidation of Mn⁴⁺ is not expected. Furthermore, 0.35 Na⁺ ions are deintercalated between 2.30 V and 3.75 V; this suggests that Ni²⁺ to Ni³⁺ oxidation is the main process in this composition range.

The plateau around 4.2 V is identified with the occurrence of biphasic domain. Fig. 6 gives a comparison of the XRD patterns of the materials recovered after one charge of the cell at 4.0 V and 4.3 V, respectively. At 4.0 V the XRD pattern is characteristic of the P2 type structure, whereas the 4.3 V one is very different. Only two main lines are observed: (i) the first one is equal to the interslab distance ($c_{\text{hex.}}/n$), (ii) the second one is characteristic of the classical intra-slab distance ($a_{\text{hex.}}$). Obviously, there is a change in the slab packing, but there is no enough data to identify the structural type. For intermediate sodium amounts in the 4.2 V plateau a mixture of both phases is observed on the XRD patterns. The length of the plateau continuously decreases upon cycling, while the capacity between 4.0 V and 2.0 V remains almost constant. In previous papers Lu et al. reported the possibility of the transition from P2 to O2 structure type for P2-Na_{2/3}Ni_{1/3}Mn_{2/3}O₂ at high voltage,³¹ while Yabuuchi et al. mentioned that in the P2-Na_{2/3}Fe_{1/2}Mn_{1/2}O₂ system the phase transition to OP4 structure type occurs by gliding of slabs at the end of the charge.¹⁴ In both cases, these structural changes result from slab gliding. In the hypothesis of the transition to O2 structure type all trigonal prismatic sites are converted to octahedral ones, whereas in the hypothesis of the transition to OP4 structure transition only 1 over 2 of those sites is alternatively transformed. In our material, it can be assumed that Na deintercalation for $x < 0.35$ leads to slab gliding with local formation of O2 type interslab spaces. It results in the formation of stacking faults that prevent a clear characterization of the material. Experiments are in progress to characterize the structure of the material obtained at high voltage. It is well-known that the stability of the trigonal prismatic vs octahedral environment of alkali ions in layered structures depends on the intercalation amount but also on the ionicity of the M-O bonds that is directly related to the slab composition see Fig. 3 in ref. 4.

As shown on Fig. 3, even if the capacity on the 4.2 V plateau decreases rapidly upon cycling, the structural defects formed during the charge seem to disappear in discharge, as the shape on the discharge curve below 4.0 V is not modified even after 10 cycles. In order to study the material stability the following experiment was done. In a first step, as shown in Fig. 7, 10 cycles were done in the 3.0–4.3 V voltage range where the phase transition occurs. The length of the

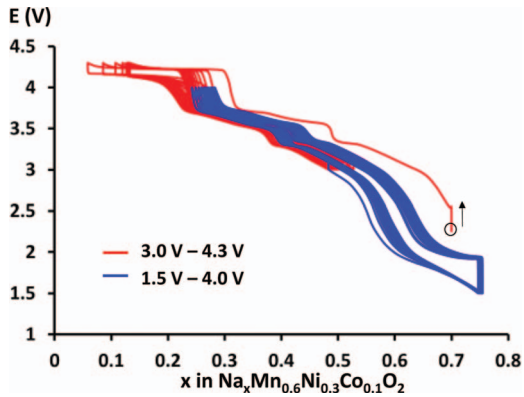


Figure 7. Effect of the cycling in the 3.0–4.3 V range on the shape of the cycling curve in the 1.5–3.0 V range.

4.2 V plateau decreases continuously. The experiment was continued with the same battery in the 1.5–4.0 V range for 10 more cycles. The shape of the curve is preserved upon cycling, which shows that no material degradation occurs during the cycling at high voltage. An XRD pattern was recorded on material recovered after 10 cycles in the 3.0–4.3 V range. At the end of the last discharge the cell voltage was maintained at 3.0 V for 24 hours to obtain a very homogeneous material. The material composition is close to $\text{Na}_{0.60}\text{Mn}_{0.60}\text{Ni}_{0.30}\text{Co}_{0.10}\text{O}_2$. Its XRD pattern (Fig. 8), typical of the P2 phase, shows that the material is well crystallized. The comparison of the cell parameters to those of the $\text{Na}_{0.70}\text{Mn}_{0.60}\text{Ni}_{0.30}\text{Co}_{0.10}\text{O}_2$ starting phase ($a_{\text{hex.}} = 2.8786(1) \text{ \AA}$ and $c_{\text{hex.}} = 11.163(1) \text{ \AA}$ for the material at 3.0 V compared to $a_{\text{hex.}} = 2.8842(1) \text{ \AA}$ and $c_{\text{hex.}} = 11.089(1) \text{ \AA}$ for the pristine material) confirms the higher average oxidation state of transition metal ions (smaller $a_{\text{hex.}}$) and the smaller amount of sodium (higher $c_{\text{hex.}}$). To determine the effect of the cycling on the particle size we selected three diffraction lines with very different Miller indexes. The comparison of the shape of the (103), (106) and (110) diffraction lines (Fig. 9) shows that there is no broadening of the (110) line, whereas there is a small broadening of the (103) and (106) ones. These lines were selected because: (i) they do not overlap with other diffractions lines (see Fig. 1), (ii) they have different Miller indexes that allows to discriminate between in slab plane and along the c axis coherence lengths. This result shows that the coherence length is maintained in the hexagonal plane, whereas it decreases slowly along the c axis that suggests the presence of some extended defects along this axis. SEM experiments after various numbers of cycles in various voltage ranges are in progress.

A capacity fading also occurs when the battery is discharged down to low voltage. Discharging the battery down to 1.5 V implies the

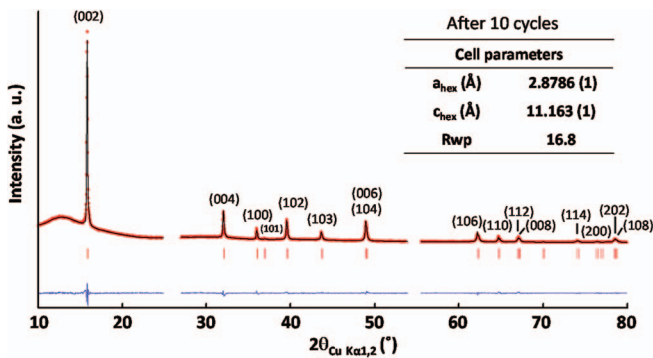


Figure 8. XRD pattern of the battery material recovered at 3.0 V after 10 cycles in the 3.0–4.3 V range: (black) full pattern matching pattern, (red) experimental data, (blue) difference plots.

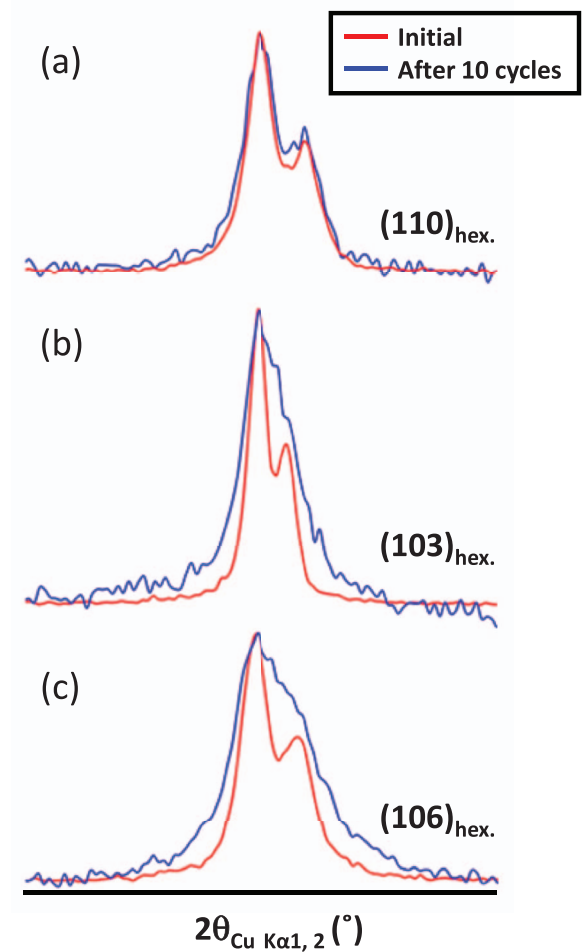


Figure 9. Comparison of the broadening of the (a) $(110)_{\text{hex}}$, (b) $(103)_{\text{hex}}$ and (c) $(106)_{\text{hex}}$ diffraction lines of the starting material (red line) and after 10 cycles in the 3.0–4.3 V range (blue line). To allow the comparison of their FWHM, the lines have been shifted along the 2θ angle; simultaneously their maximum has been normalized.

reduction of Mn^{4+} to Mn^{3+} in a larger amount than for a discharge down to 1.7 V. It is assumed that the existence of Mn^{3+} ions leading to the Jahn-Teller distortion of MnO_6 octahedra, which can induce constraints and defects in the material that may increase the capacity fading.

Conclusions

$\text{P2-Na}_{0.70}\text{Mn}_{0.60}\text{Ni}_{0.30}\text{Co}_{0.10}\text{O}_2$ was synthesized using the co-precipitation method. To get a pure P2 phase, it is required to avoid Ni^{3+} in the targeted composition. Therefore, the composition was determined to have only Ni^{2+} in the pristine material. This material delivers 185 mAh/g as maximum specific capacity. In the voltage plateau indicating bi-phase transition around 4.2 V, it can be assumed that O2 type stacking faults occurred within the P2 structure. Although the capacity retention after 20 cycles in the 1.5–4.3 V range is only 58%, it could achieve high cycle retention (94%) when the cut-off voltage is limited in 1.7–4.0 V. The reason of this capacity fade either in charge or in discharge is not clear. XRD study after 10 cycles in the high voltage range, where the fading is quite large, shows that the crystallinity on the structure is preserved. Further investigations are in progress to understand the relationships between electrochemical properties and structural changes.

Acknowledgments

The authors thank C. Denage for technical assistance and Toyota, CNRS and Region Aquitaine for financial support.

References

1. C. Delmas, J.-J. Braconnier, C. Fouassier, and P. Hagenmuller, *Solid State Ionics*, **3-4(C)**, 165 (1981).
2. C. Delmas, J.-J. Braconnier, A. Maazaz, and P. Hagenmuller, *Revue de Chimie Minerale*, **19**, 343 (1982).
3. J. J. Braconnier and C. Delmas Et P. Hagenmuller, *Mat. Res. Bull.*, **17**, 993 (1982).
4. C. Delmas, C. Fouassier, and P. Hagenmuller, *Physica*, **99B**, 81 (1980).
5. Z. Lu and J. R. Dahn, *J. Electrochem. Soc.*, **148(11)**, A1225 (2001).
6. J. M. Paulsen and J. R. Dahn, *J. Electrochem. Soc.*, **147(7)**, 2478 (2000).
7. Z. Lu, R. A. Donaberger, and J. R. Dahn, *Chem. Mater.* **12**, 3583 (2000).
8. Z. Lu, R. A. Donaberger, C. L. Thomas, and J. R. Dahn, *J. Electrochem. Soc.*, **149(8)**, A1083 (2002).
9. J. Xu, D. Lee, and S. Meng, *Funct. Mat. Letters*, **6(1)**, 1330001 (2013).
10. M. Slater, D. Kim, E. Lee, and C. Johnson, *Adv. Funct. Mater.*, **23**, 947 (2013).
11. V. Palomares, M. Casas-Cabanas, E. Castillo-Martinez, M. Han, and T. Rojo, *Energy Environ. Sci.* **6**, 2312 (2013).
12. H. Pan, Y.-S. Hu, and Liqun Chen, *Energy Environ. Sci.* **6**, 2338 (2013).
13. S. Kikkawa, S. Miyazaki, and M. Koizumi, *Journal of Power Sources*, **14**, 231 (1985).
14. N. Yabuuchi, M. Kajiyama, J. Iwatate, H. Nishikawa, S. Hitomi, R. Okuyama, R. Usui, Y. Yamada, and S. Komaba, *Nature Materials*, **11**, 512 (2013).
15. B. Mortemard de Boisse, D. Carlier, M. Guignard, and C. Delmas, *J. Electrochem. Soc.*, **160(4)**, A569 (2013).
16. J. S. Thorne, R. A. Dunlap, and M. N. Obrovac, *J. Electrochem. Soc.* **160(2)**, A361 (2013).
17. D. H. Lee, J. Xu, and Y. S. Meng, *Phys. Chem. Chem. Phys.*, **15**, 3304 (2013).
18. H. Wang, B. Yang, X.-Z. Liao, J. Xu, D. Yang, Y.-S. He, and Z. F. Ma, *Electrochemical Acta*, **113**, 200 (2013).
19. D. Carlier, J. H. Cheng, R. Berthelot, M. Guignard, M. Yoncheva, R. Stoyanova, B. J. Hwang, and C. Delmas, *Dalton Trans.* **40**, 9306 (2011).
20. N. Bucher, S. Hartung, I. Gocheva, Y. L. Cheah, M. Srinivasan, and H. E. Hoster, *J. Solid State Electrochem.*, **17**, 1923 (2013).
21. D. Buchholz, A. Moretti, R. Kloepsch, S. Nowak, V. Siozios, M. Winter, and S. Passerini, *Chem. Mater.* **25**, 142 (2013).
22. D. Yuan, W. He, F. Pei, F. Wu, Y. Wu, J. Qian, Y. Cao, Z. Ai, and H. Yang, *J. Mater. Chem.* **1**, 3895 (2013).
23. S. Doubaji, M. Valvo, I. Saadoune, M. Dahbi, and K. Edström, *J. Power Sources*, **266**, 275 (2014).
24. T. Ohzuku and Y. Makimura, *Chem. Lett.*, **30**, 642 (2001).
25. D. Yuan, X. Hu, J. Qian, F. Pei, F. Wu, R. Mao, X. Ai, H. Yang, and Y. Cao, *Electrochimica Acta*, **116**, 300 (2014).
26. T. Roisnel and J. Rodríguez-Cravajal, *Materials Science Forum*, **378-381**, 118 (2001).
27. F. Weill, N. Tran, L. Croguennec, and C. Delmas, *Journal of Power Sources*, **172**, 893 (2007).
28. S. Komaba, T. Ishikawa, N. Yabuuchi, W. Murata, A. Ito, and Y. Ohsawa, *ACS Appl. Mater. Interfaces*, **3**, 4165 (2011).
29. J.-H. Cheng, C.-J. Pan, J.-F. Lee, J.-M. Chen, M. Guignard, C. Delmas, D. Carlier, and B.-J. Hwang, *Chem. Mater.* **26**, 1219 (2014).
30. R. Berthelot, D. Carlier, and C. Delmas, *Nature Materials*, **10**, 74 (2011).
31. Z. Lu and J. R. Dahn, *J. Electrochem. Soc.*, **148(7)**, A710 (2001).